

# EFFECT OF POPULAR ADDITIVE MANUFACTURING TECHNOLOGIES ON THE PERFORMANCE AND ACOUSTICS OF UAV PROPELLERS

J. García-Tíscar<sup>1</sup>, P. Quintero<sup>1</sup>, F. N. Ramírez<sup>1</sup> & A. Cremades<sup>2</sup>

<sup>1</sup>CMT – Clean Mobility & Thermofluids, Universitat Politècnica de València, Valencia, Spain <sup>2</sup>FLOW, Engineering Mechanics, KTH Royal Institute of Technology, Stockholm, Sweden

#### **Abstract**

UAV noise remains a major concern for the widespread implementation of these aircraft in a wide array of potential applications, especially in the urban environment. Moreover, not only overall noise levels must be considered when analyzing the impact of UAV noise; noise quality based on the spectral content of the acoustic signal must be considered due to the psychoacoustic impact on the listeners. Also, as UAVs become widespread, the ability to perform field replacement of propellers using additive manufacturing (AM) is of increased interest to many operators. However, as different AM techniques become popular, their impact on performance and noise must be assessed. In this investigation, we experimentally test the same propeller geometry manufactured using the most popular AM techniques, evaluating how different characteristics such as surface roughness, anisotropy, and flexibility affect the propeller. Finally, we performed a numerical campaign to isolate these effects and better understand their effect on propeller noise and performance.

Keywords: Acoustics, Drones, Computer Fluid Dynamics

## 1. Introduction

Unmanned Air Vehicles (UAVs) popularity as an aerial platform for a wide range of civil and military applications keeps increasing. From recreative purposes to surveillance and fire safety, passing through filmmaking, infrastructure inspection, road traffic control, cell network augmentation, and so on, these aircraft are becoming widespread in both the countryside and urban spaces [1].

However, even though the technology in terms of flight performance is mature, its full potential given all these applications is not yet fully realized, partly due to a combination of regulative, safety, and acceptability concerns. On the first two fronts, several initiatives in the US, EU, UK, etc., aim to achieve a harmonized regulation that allows the safe operation of UAVs [2, 3]. However, some concerns remain regarding the public acceptability of UAV operations. Public opinion surveys conducted by aviation authorities have found that UAV noise is one of the leading factors among these concerns [4].

When considering UAV noise, two aspects come into play. On the one hand, there is the issue of overall noise level. This is simply the added global level that continued UAV operation could bring into homes, schools, hospitals, etc. As per WHO findings, noise levels are the second most harmful form of environmental cause of health problems, just after chemical pollutants [5]. Thus, care should be taken to ensure that the new services afforded by UAVs do not increase these noise levels and their health consequences for the population. On the other hand, the psychoacoustic impact of UAV noise signatures has been attested. Due to the particular flight dynamics of UAVs, based on multipropeller speed control, the frequency content of the noise presents a semi-random variance around an average, often perceived as especially annoying [4, 6]. Therefore, both overall noise levels and frequency content must be studied to address these concerns properly.

In parallel with UAVs, another technology that is becoming widespread is Additive Manufacturing (AM). Since UAVs are often subjected to crashes or forced landing, which may imply a degree of damage, and given that the propellers are often the most easily damaged part, rapid in-field replacement of these components becomes an extremely desirable capability for many kinds of operators,

both civil and military. For example, UAVs are being used to deliver medical supplies in remote locations where land-based communications are scarce and difficult [7], deployed on the battlefield, or even embarked in ocean-going naval units [8]. Obtaining spare parts such as propellers from the UAV manufacturer is difficult or impossible in these situations, and thus, the ability to rapidly manufacture any required spare from a supply of raw material becomes highly desirable.

However, replacing a commercial propeller with a 3D-printed one is not straightforward, even if the geometry is exactly the same. As different AM techniques result in pieces with distinct mechanical properties such as flexibility, surface finish, roughness, anisotropy, etc., there is no guarantee that the performance of a recreated propeller, in terms of thrust, torque, and noise emission, is equivalent to that of the original. The effect of FDM and SLA propellers has been previously studied experimentally [9], focusing on the effect of surface roughness on performance, vibrations, and overall sound pressure level. Moreover, performance and acoustic comparisons of SLA and SLS propellers have been carried out [10]. However, further research is still needed to determine the influence of the material properties on the performance and noise emission. In addition, an analysis of the influence of these parameters on the full acoustic spectra is missing in the literature. To address this issue, in this investigation, we consider one wooden commercial propeller typical of UAVs and recreate it using the three most widespread AM techniques. We test these propellers in our anechoic test bench to assess the impact of the different AM methods on thrust, torque, and noise emission, including overall level, directivity, and spectral content. Since each technique introduces its particular combination of mechanical properties, we then perform a numerical simulation campaign in which we modify each mechanical property separately, allowing us to better understand their impact on the propeller performance.

# 2. Methodology

## 2.1 Selected propeller

The commercial wooden XOAR PJN 9x7" (22.86 cm) propeller was selected for this investigation. This kind of propeller is typical of fixed-wing UAVs such as the VALAQ120 by the UAV Works Group. In order to create the additive-manufactured (AM) versions of the propeller and be able to carry out the numerical simulations, a digital model was first obtained using a structured-light 3D scanner. The scanning was not without imperfections, and thus, a manual postprocessing was required. Since the scanner did not correctly capture one of the blades' trailing edges, the other blade was duplicated and mirrored. The shaft hole also had to be recreated manually for the 3D-printed pieces. Figure 1 depicts the aforementioned process.

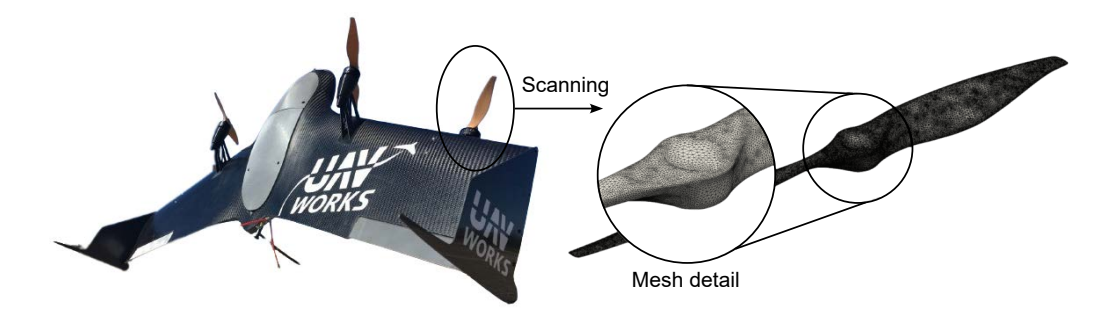


Figure 1 – Overview of the propeller placement on a UAV and the result of the scanning process.

## 2.2 Additive manufacturing

The term Additive Manufacturing (AM), also known popularly as 3D printing, encompasses a large variety of very different technologies. Each technology has its own strong points and weaknesses, especially in terms of mechanical properties and surface finish of the resulting items. In this investigation, we have selected three of the most popular, which are briefly described in this subsection. Because the COTS propeller broke after the scanning process, only the results of the 3D printed propellers are shown in the present work. By generating the three tested experimental geometries

from the obtained stl, part of the experimental uncertainty due to possible errors in the scanning is also reduced.

# 2.2.1 Fused Deposition Modeling (FDM)

Fused Deposition Modeling (FDM), also known as Fused Filament Fabrication (FFF), is probably the most well-known AM technology and can be considered as the one kickstarting its recent popularity surge. In its essence, a continuous filament of thermoplastic material is extruded through a heated printing head, which causes the material to melt or soften enough to fuse with the previously deposited material. The extruder head is continuously moved as required to form the geometry of the desired item.

The movements of the extruded heads are pre-computed through a software called *slicer*, because the typical approach is to "slice" the item geometry into a series of horizontal planes. The head will complete all the required XY movements in each Z plane before moving to the next one, which is typically accomplished by lowering the building platform itself. A schematic of the manufacturing process can be seen on the left of Figure 2. This process results in a manufactured item that clearly shows the different Z layers in its surface finish, in addition to possible "Z seams" resulting from the filament extrusion's starting and finishing points at each layer. Moreover, the overhanging parts of the geometry require supporting material that needs to be removed in postprocessing steps.

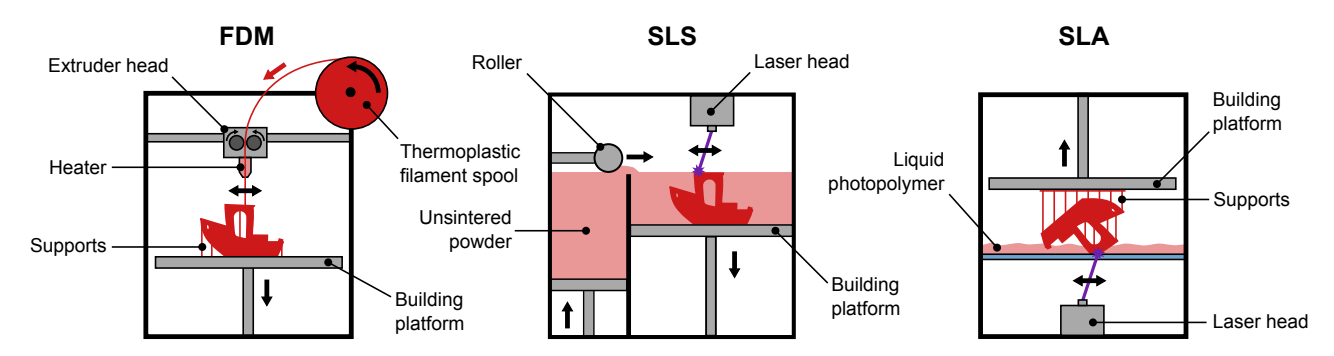


Figure 2 – Conceptual schematic of AM technologies used in this research.

In addition, the process of building the object through subsequent Z layers of fused or deposited cordons of thermoplastic filament results in anisotropic mechanical properties, as the behavior in the Z direction is usually quite different from that of the X and Y directions. Furthermore, objects are not fully filled even if 100% infill is selected, as the 3D space cannot be filled by the cylindric geometry of the filaments.

## 2.2.2 Selective Laser Sintering (SLS)

SLS technology solves many of these issues. In this approach, a high-power, orientable laser melts small particles of the building material (typically a polyamide such as PA11 or PA12), fusing them together to form a solid object. Again, the process involves slicing the object into Z planes, as the laser can only traverse the XY plane. Powdered material from a reservoir is thinly spread over a movable bed, where the laser sinters the required slice. Then, the bed is lowered, a fresh, unsintered powder layer is spread on top, and the process repeats until the object has been fully built. A schematic of this process is shown in the center image of Figure 2.

This technique presents several advantages. First, the resulting object has practically isotropic mechanical properties, as the powder particles have fused together. Also, the surface resolution is better than with the FDM process, as it is not limited by the geometry of the deposited filaments. Finally, as the sintered material is supported by the unsintered powder, no support material is required. In fact, very complex and interlocking geometries can be produced by taking advantage of this fact.

However, this method is not without disadvantages. First and foremost, the requirement of a high-powered laser increases the complexity and cost of the machine, restricting its use to more professional settings rather than hobby or household environments. Working with powdered material can also be a nuisance, and require procedures and/or a dedicated workshop. The surface finish is usually rough, even if it is free of visible Z layers or seams.

# 2.2.3 Stereolithography (SLA)

Finally, the SLA technique relies on the photopolymerization of resin. When a UV laser is focused on the bottom of a vat containing photopolymer resin, the resin solidifies through a photochemical process. The laser is steered to solidify the Z slice as required, and then, the liquid vat is lowered and the laser draws the next slice, which is fused with the previous one. This process is illustrated on the right side of Figure 2.

Through this process, no layering or seams are typically produced. Also, the resulting pieces exhibit isotropic mechanical properties. Nowadays, SLA machines can be more accessible than SLS ones. Furthermore, a wide array of resins with different properties are available, although the material choice is not as varied as with FDM. A variant of this technique uses a projector to shine the complete image of each slice into the resin vat, which lowers the cost of the machine even more. These are known as Digital Light Processing (DPL) machines. However, the projects work by projecting a raster image (made up of pixels) instead of the continuous movement of the laser spot of SLA machines. Thus, DPL produces pieces exhibiting a certain voxel effect, as if constructed of tiny cubes.

While SLA presents certain advantages, it also has some drawbacks. Working with the photopolymer can be difficult, and certain precautions must be taken to handle it. The resulting "green" pieces must be cleaned of liquid resin that has failed to solidify. Then, the pieces must be cured with a combination of temperature and UV light in order to attain their best mechanical properties. Also, similarly to FDM, the pieces often require support as they are being built. However, unlike with FDM in which an auxiliary extruder can provide a specialized, soluble support material, the supports in SLA need to be made of the resin available in the vat. When removing the supporting struts, some marks may remain on the surface of the piece, requiring manual sanding.

## 2.2.4 Facilities and materials

For this research, the FDM propeller was manufactured in Acrylonitrile Butadiene Styrene (ABS-M30) thermoplastic using a Stratasys F170 machine. The Z layer resolution was 125  $\mu$ m, with the propeller being printed in layers parallel to the rotation plane. 100 % infill was selected in the slicer software. A limonene-soluble support material was also used to ensure proper attachment, which was removed in postprocessing.

The SLS propeller was manufactured using a Formlabs Fuse 1 system. It features a 10 W ytterbium laser and is capable of a layer resolution of 110  $\mu$ m, with a laser focal point of 200  $\mu$ m. The employed material was Nylon 12. This is the only technology that required no supports or postprocessing other than cleaning the unsintered powder.

Finally, the SLA propeller was created with a Formlabs 3L printer. This machine features a variant of the SLA method called Low Force Stereolithography (LFS), which uses a roller and a flexible tray floor in order to ensure that only a very thin layer of resin is cured by the laser. Two 250 mW laser heads are used to speed up the process. The selected layer height was 50  $\mu$ m and the XY resolution was 25  $\mu$ m, while the standard Formlabs Grey v4 resin was used. The propeller was then cleaned with



Figure 3 – The propellers tested in this investigation. From left to right: original wooden propeller, FDM, SLS and SLA-manufactured versions.

isopropyl alcohol and cured with the temperature and UV light cycles prescribed by the manufacturer. The support marks were manually sanded off.

In Fig. 3, the original wooden propeller is compared against the resulting propellers manufactured by each of the selected technologies. It can be seen how the FDM propeller features very clear layers, along with the paths of the filament (note especially how the shaft wall is created by a circular filament deposition). The SLS propeller does not show any inhomogeneity, but a rougher surface can be clearly appreciated. Finally, the SLA propeller shows a smooth surface finish, appearing similar to a cast plastic piece. Focusing on the material properties, Table 1 displays the main mechanical properties of the materials used in this study according to the manufacturers.

T		1 1949		and the second of the second
Table 1 – Mechanical	nronerties of the	additive manutactu	rına materials	used in this stridy
iable i wiconanica		additive illalialacta	inig materials	acca iii tiilo otaay

Property	Unit	FDM: ABS-M30	SLS: Nylon 12	SLA: Grey v4 (PC)	
Tensile modulus XZ	GPa	2.4	4.05	2.8	
Tensile modulus ZX	GPa	2.3	1.85		
Flexural modulus XZ	GPa	2.22	1.6	2.2	
Flexural modulus ZX	GPa	1.96	1.6		
Ultimate tensile strength XZ	MPa	28.1	E0	65	
Ultimate tensile strength ZX	MPa	26.8	50		
Flexural strength XZ	MPa	-	66	-	
Flexural strength ZX	MPa	47.7	00		
Tens. elongation at break X/Y	%	8.1	11	6	
Tens. elongation at break Z	%	1.8	6		
Heat Deflection Temp 0.45 Mpa		103.8	171	73	
Heat Deflection Temp 1.8 Mpa	ºC	99.9	87	58	

#### 2.3 Test bench

In order to measure simultaneously the aerodynamic performance and the noise emission of each propeller, a custom force-measurement test bench was installed in the anechoic chamber available at Laboratory 5K of the CMT Institute. This chamber features a frequency cut-off of 100 Hz, and an available interior space of  $7.5 \times 6.5 \times 6$  m.

A schematic of the experimental setup can be seen in Fig. 4. Approximately in the middle of the chamber, a test bench featuring three load cells measures both the thrust generated by the propeller (via a 10 kg WIKA F4801 load cell) and the torque (via two 1 kg WIKA F4802 load cells). The engine is an Avenger V3 2812-900 kv, and is governed by a V-GOOD 2-6S 40A Electronic Speed Controller (ESC). An Arduino UNO microcontroller, linked to a computer in the control room, commands the ESC and also acquires the load cells' readings through three HX711 amplifiers. An optical tachometer is also read by the microcontroller in order to ensure the desired rotating speed.

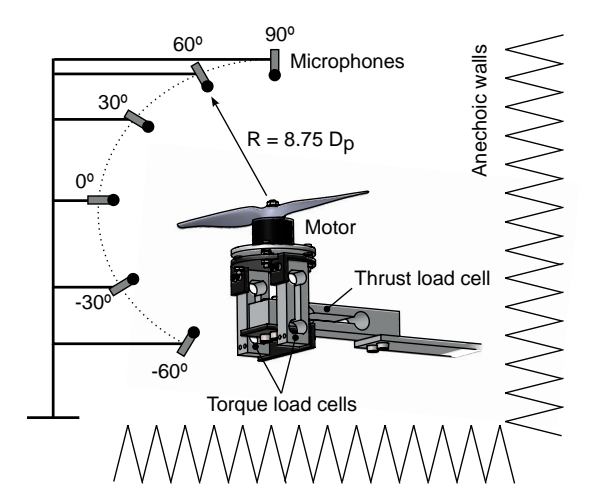




Figure 4 – Schematic of the experimental setup and Anechoic chamber at the CMT Institute.

To measure the acoustic emission, six Brüel & Kjær Type 4190 free-field microphones are mounted in an arch, at a distance from the propeller hub of 2 meters, or 8.75 propeller diameters  $(D_p)$ . The six microphones are mounted in increments of  $30^{\circ}$ , starting from the vertical (upstream) of the propeller. They are simultaneously acquired by a PULSE Type 3560-D Data Acquisition System from Brüel & Kjær, also linked to the control room computer.

After calibrating the load cells with reference weights and the microphones through a Brüel & Kjær Type 3541 pistonphone, measurements were made at different speeds, capturing the acoustic signal for 2 seconds and the force variables for at least 60 seconds. At least three repetitions of the measurements were conducted for each propeller to ensure repeatability. The covered speed range comprised from 3900 to 12000 RPM, corresponding to a tip Mach between 0.1373 and 0.4225.

# 2.4 Numerical setup

In order to better understand the role of surface roughness and flexing under load on both aerodynamic and acoustic performances, a numerical experiment was carried out, where advantage was taken of a previously validated numerical setup for a rigid, smooth propeller previously described by Serrano et al. [11]. In this work, the simulations were performed following the same approach but using the commercial software *SimCenter STAR-CCM+* 2210.

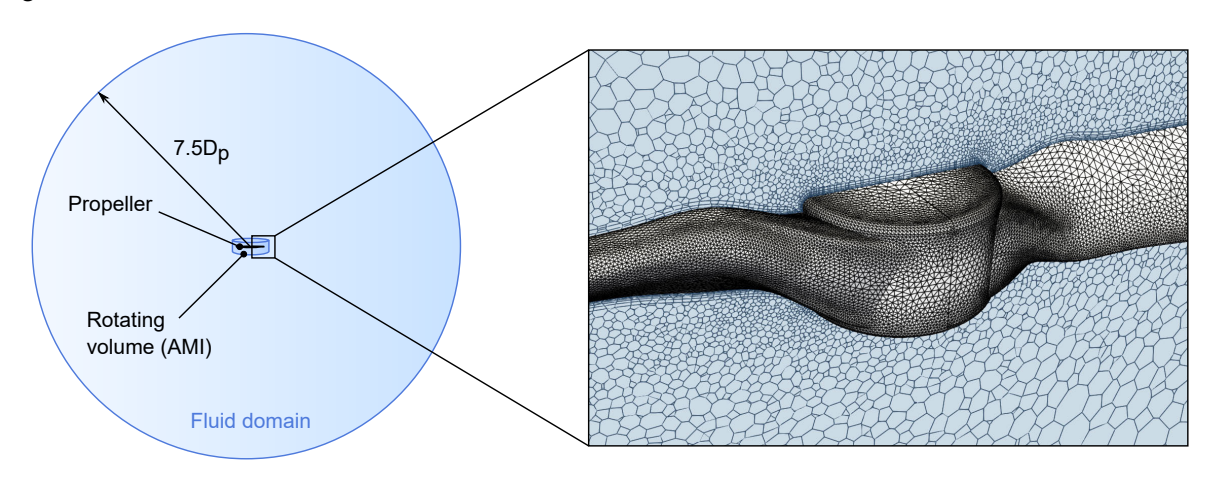


Figure 5 – Numerical domain of the simulations together with a mesh snapshot.

As can be seen in Fig. 5, only the propeller is modeled. It is immersed in a spherical fluid domain with a radius of  $7.5D_p$ . A rotating mesh approach is used, with the rotating domain defined as a small cylinder around the propeller. The mesh totals  $\sim$ 2.5 million cells, 500k of them for the blade solid domain and the rest for the fluid domain.

The first main modification of the existing model for this investigation was the consideration of Fluid-Structure Interaction (FSI), solving a Finite Element Model (FEM) of the propeller in coupling with the finite-volume fluid solver. This way, it is possible to modify the Young's modulus of the propeller to study how this feature impacts the performance of the isolated propeller.

The second modification will consist of introducing a variable wall roughness via a corrected wall function to sweep this parameter and assess its influence on performance. This will allow us to study the effect of both parameters in isolation in order to better understand the experimental data, in which these parameters cannot be easily changed individually as they are characteristic of each selected AM technique. For this purpose, simulations at 9870 rpm have been carried out varying the Young's modulus and surface roughness.

Following a dimensional analysis similar to the one performed by Torregrosa et al. ([12], [13]), the torque (Q), aerodynamic power (P) and thrust (T) can be normalized characterizing the blade by its torque coefficient  $(C_Q)$ , power coefficient  $(C_P)$  and thrust coefficient  $(C_T)$ , whereas E can be similarly normalized to  $E^*$  as shown in Equation 1, where  $\rho_{\infty}$  represents the undisturbed air density, n is the rotational speed of the blade in rev/s and D is the diameter of the propeller.

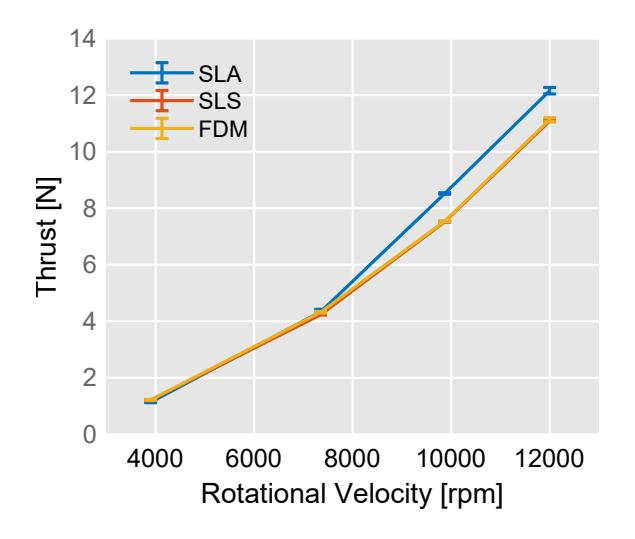
$$C_Q = \frac{Q}{\rho_{\infty} n^2 D^5}$$
  $C_P = \frac{P}{\rho_{\infty} n^3 D^5}$   $C_T = \frac{T}{\rho_{\infty} n^2 D^4}$   $E^* = \frac{E}{\rho_{\infty} n^2 D^2}$  (1)

## 3. Results & discussion

## 3.1 Experimental campaign

After manufacturing the different propellers using the AM technologies described in section 2.2 these were installed and tested in the anechoic chamber test bench, where the raw readings from the load cells and microphones were recorded. As stated before, at least three repetitions of the measurements were performed for each propeller.

Using the load cell calibrations performed before the measurement, the time evolution of thrust and torque during the experiments was obtained. For each propeller speed, the average of the thrust and torque signals were computed, and the standard deviation between measurements was obtained, with the results being shown in Fig. 6. It can be observed that at low rotational speeds, there is no significant difference in thrust between propellers, while as the rotational speed increases, there is a substantial increase in the performance of the propeller made of SLA with respect to the other two propellers, the bigger difference found is about a 13% at 9870 rpm. Since this difference is highly dependent on the rotation regime, it seems to be due to aeroelastic phenomena produced by the difference in the materials' flexibility. This would imply that the SLA propeller has a lower Young's modulus than expected from Table 1, or that in the other propellers the material effect is masked by the effect of surface roughness.



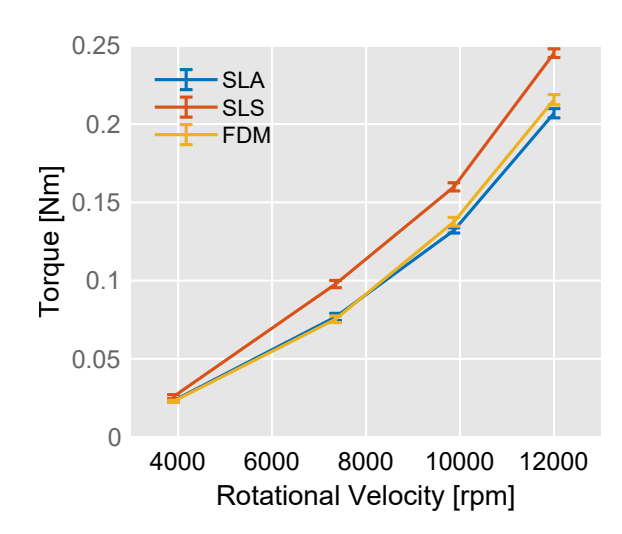


Figure 6 – Thrust and torque in hover of each of the considered propellers.

On the other hand, the propeller manufactured with SLS is the one that generates the highest torque, this difference being appreciable at all rotational speeds, so it can be presumed that this phenomenon occurs mainly due to the difference in the surface finish (rugosity) of the propellers. This is expected since the superficial finish of the SLS propeller, although homogeneous, is highly textured. The other two propellers generate a similar torque, with the FDM propeller slightly higher than the SLA one at high speeds. SLA and SLS propellers' trends are consistent with results found in the literature [10]. It can be seen that the two factors that have the greatest effect on performance (material and surface finish) operate simultaneously, making it impossible to discern the effect of each one on the performance clearly. For this reason, a numerical investigation will be carried out to confirm the findings obtained and to acquire a deeper understanding of the underlying phenomena.

As for the noise generated by each of the propellers manufactured with AM, the frequency spectra obtained around the propeller at different angles and a radius of 2 meters and 9870 rpm are shown in Figure 8. It can be observed that at the first blade passing frequency (330 Hz), the sound level achieved is very similar among the three propellers, being slightly higher for the SLS propeller than for the other two. This is shown in more detail in Fig. 7 (left). This sound increase is also observed, with greater amplitude, in the broadband noise at higher frequencies (1000 – 10 000 Hz), where it can be seen how the SLS propeller generates a considerable noise increment, presumably due to the surface finish which presumably leads to a fully turbulent boundary layer and, therefore, to an increase of turbulence-related noise. This increase in broadband noise has a considerable impact on the overall noise, as can be seen in Fig. 7 (right).

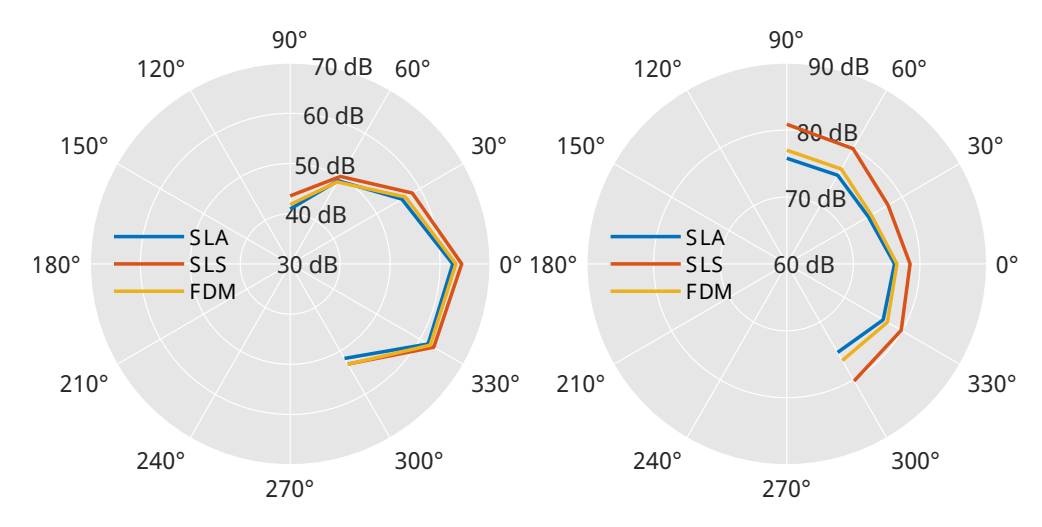


Figure 7 – Sound Pressure Level at the Blade Passing Frequency (left) and Overall Sound Pressure Level (right) directivity of the propellers at 9870 rpm.

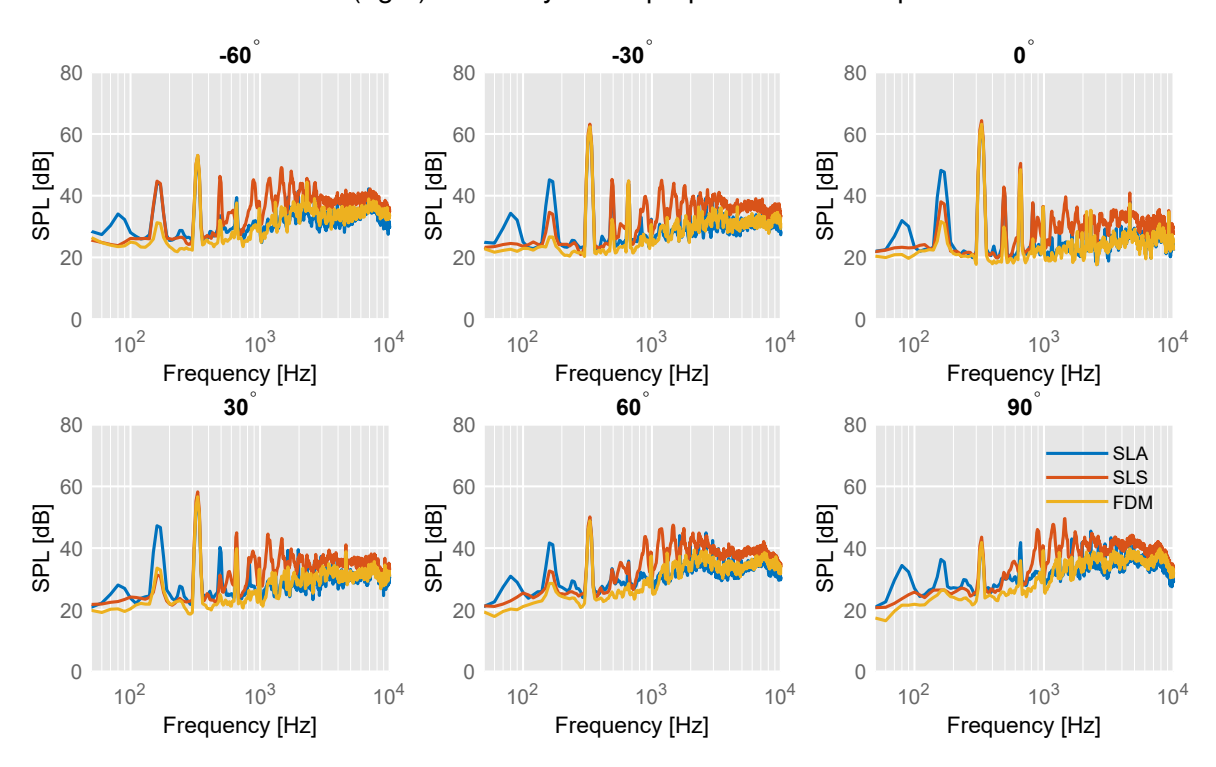


Figure 8 – Frequency spectrum at each of the six microphone positions at 9870 rpm.

In addition, it can be observed how a peak appears at the shaft frequency (half the first blade passing frequency) for the three propellers. This peak is higher in the case of the propeller manufactured in SLA, which would indicate that this propeller has the greatest geometrical asymmetry between blades. This is probably due to the effect of hand sanding on the geometry.

Finally, in Fig. 8, it can be observed a new peak arising at 80 Hz for the SLA propeller. This low-frequency peak does not correspond to any expected acoustic source and is believed to be caused by the presence of aeroelastic phenomena. This hypothesis will be supported by the results of the numerical simulations shown in the following section.

#### 3.2 Numerical results

As for the numerical analysis, simulations were carried out assuming isotropic materials and with different surface roughness to distinguish the effect of each of those factors.

The deformation of the propeller is one of the most representative forms for understanding the importance of FSI and aeroelastic couplings. Specifically, two of the most representative values are the

tip displacement,  $\delta$ , and the tip torsion,  $\Delta\theta$  [14]. In Figure 9, the deformed propeller colored by the displacement distribution is shown for a zero surface roughness propeller with Young's modulus of E=1 Gpa at 9870 rpm.

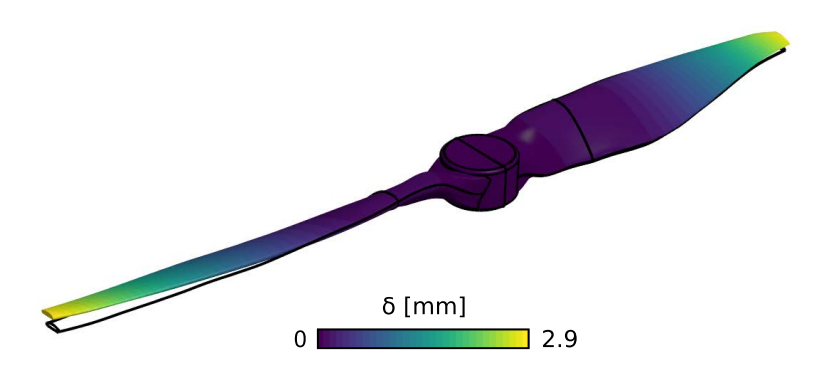


Figure 9 – Deformed propeller colored by displacement magnitude at 9870 rpm with E = 1 GPa

In Figure 10, tip displacement (left) and tip torsion (right) as a function of the non-dimensional stiffness parameter  $E^*$ , and for four different surface roughness are shown. It can be observed that, for the smooth propeller, a reduction of E, which corresponds with a reduction of  $E^*$  if n is constant, implies an increase in both parameters, as expected. Regarding the influence of surface roughness, it can be observed that the inclusion of its effect reduces the influence of the material, reducing both deformations. Moreover, the difference between a relatively small roughness ( $\mu=0.20$  mm) and a big one ( $\mu=1.00$  mm) isn't significant.

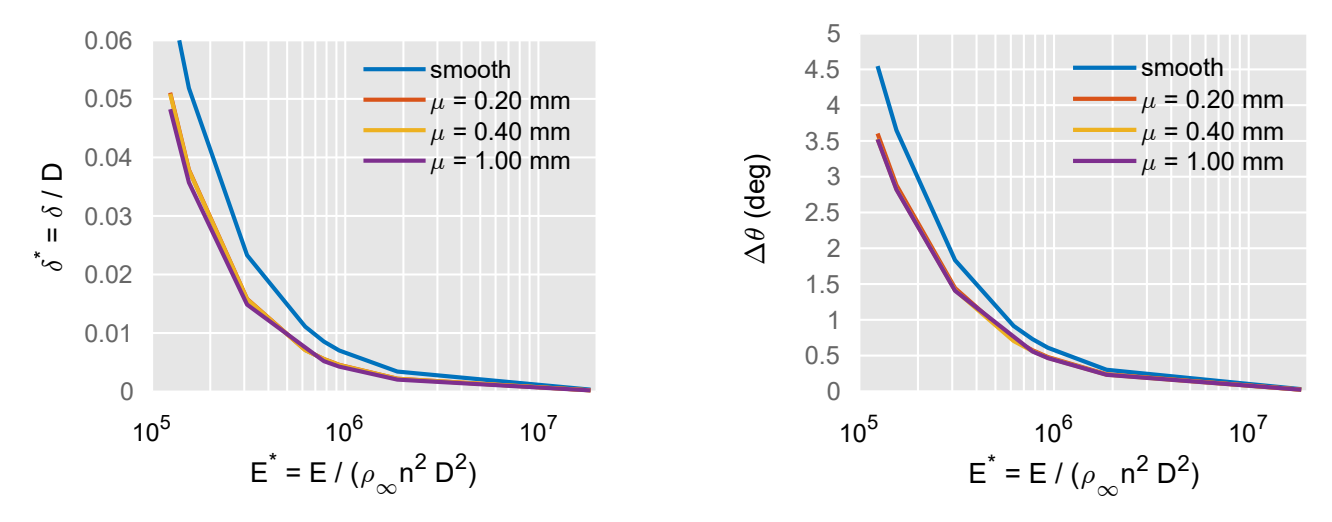
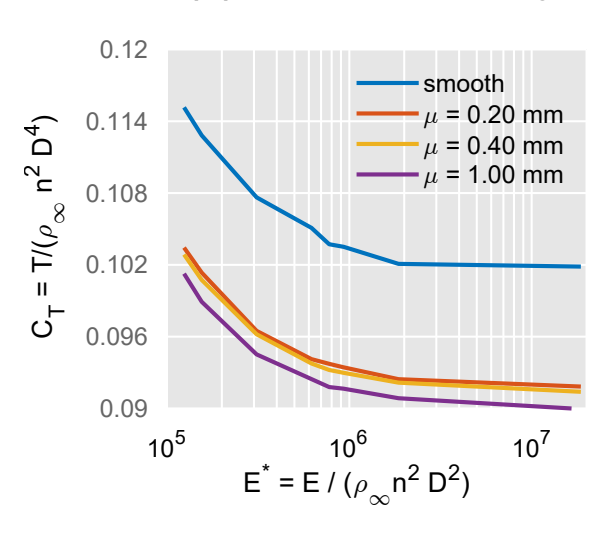


Figure 10 – Numerical prediction of non-dimensional tip displacement (left) and tip torsion (right) in hover varying the Young's Modulus for different surface roughness.

On the other hand, it is also of interest to determine if the inclusion of the material effect could be related to a significant change in the aerodynamic features of the blade. In order to quantify this, Figure 11 shows the thrust and torque coefficient as a function of the non-dimensional stiffness parameter. For the smooth case, it can be seen that at high Young's modulus, the rotational velocity doesn't have a significant impact on the non-dimensional coefficients, while reducing Young's modulus results in an increase in both thrust and power coefficients (with a higher increase in power), as well as a greater dependence on the rotational speed, as assumed from the experimental results. Regarding the surface roughness, a greater dependence on the  $\mu$  value is found, although the biggest difference still appears between low  $\mu$  values and the smooth propeller with a 9.9% thrust variation and a 7.9% power difference between the smooth propeller and the  $\mu=0.2$  mm case. Again, the difference between low and high values of  $\mu$  does not represent a significant change.

Figure 12 shows the time evolution of the tip displacement for different Youngs' modulus values (left) and the frequency spectra of said time evolution. It can be seen that the deformation at the tip hap-



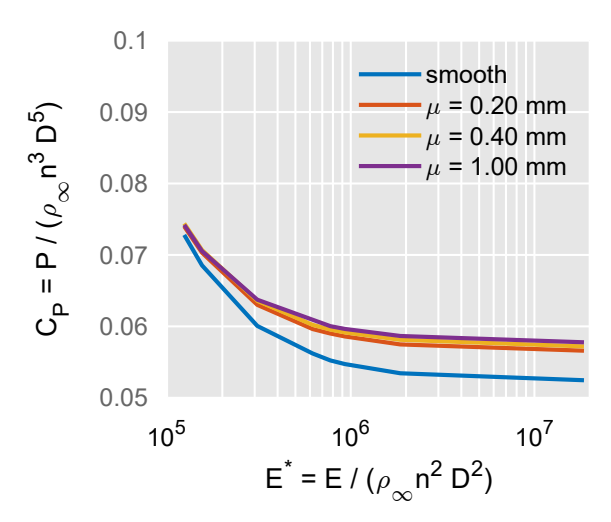
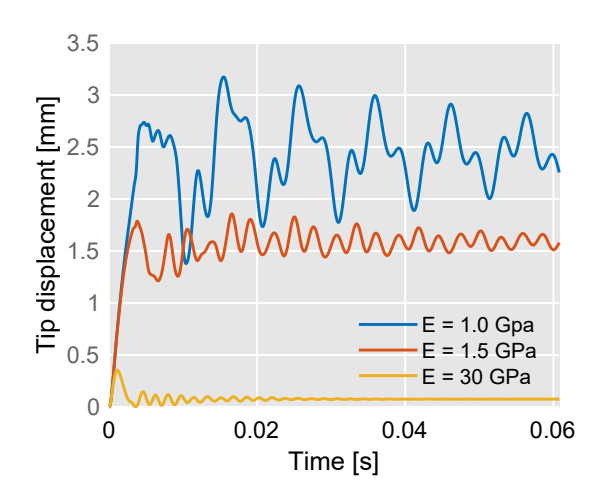


Figure 11 – Numerical prediction of thrust coefficient (left) and power coefficient (right) in hover varying the Young's Modulus for different surface roughness.

pens at specific frequencies, which depends on the material of the propellers. These peaks became relevant at E=1.0 GPa, where it appears at 100 Hz. This observation matches the previous hypothesis, where it was speculated that the peak at 80 Hz in the SLA propeller was due to aeroacoustic phenomena. This also implies that the SLA propeller has a lower Young's modulus than expected, as stated in subsection 3.1.



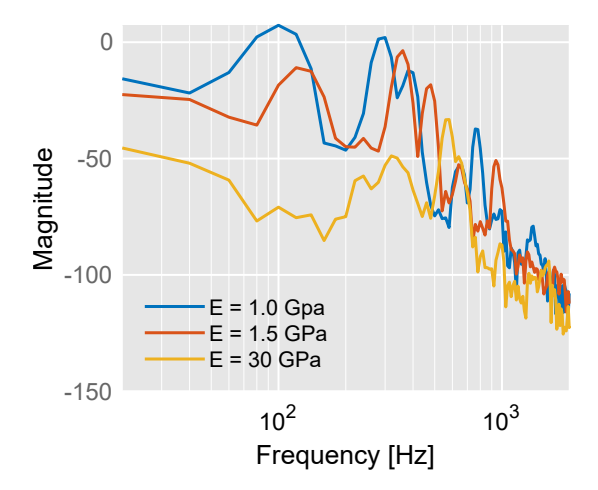


Figure 12 – Time evolution and frequency spectra of tip displacement.

## 4. Conclusions and future work

In this work, the influence of three different additive manufacturing technologies (FDM, SLA, and SLS) on the performance and noise emission of small-diameter propellers has been investigated. The SLS propeller has been found to be the least efficient and loudest, while the SLA propeller presented the best thrust/torque relation at hover with the lowest noise emissions.

A numerical study was carried out to study the influence of the effect of the material and the surface roughness as isolated and combined effects. It was found that smaller Youngs' modulus results in an increase in thrust but a reduction of the mechanical efficiency of the propeller (due to a higher increase in torque). This can be clearly seen in Table 2, where the results for different values of E for the smooth case are shown.

Moreover, it has been observed that, at very small values of E, aeroelastic phenomena may produce tonal noise at low frequencies that are not relevant for rigid propellers.

On the other side, the numerical results showed that a surface roughness increase leads to a reduction in thrust and an increase in torque. This effect is more relevant between the smooth propeller and small values of  $\mu$ , and flatten out for relatively high values, as can be shown in Table 3.

#### Effect of popular additive manufacturing technologies on the performance and acoustics of UAV propellers

E [GPa]	0.20	0.25	0.50	1.00	1.25	1.50	3.00	30.00
Thrust [N]	9.40	9.21	8.79	8.58	8.47	8.45	8.33	8.31
Power [W]	219.94	207.05	181.44	169.80	166.85	165.31	161.43	158.48

Table 2 – Thrust and power values with different Youngs' moduli for the smooth case.

$\mu$ [mm]	0.00	0.20	0.40	1.00
Thrust [N]	8.31	7.49	7.46	7.34
Power [W]	158.48	170.98	172.79	174.53

Table 3 – Thrust and power values at different surface roughness for the E = 30 GPa case.

Further work includes adding experimental measurements of more propellers (ABS with different layer heights, different resins, etc.), an extension of the numerical results, computing the acoustic emissions (through the Ffowcs-Williams & Hawkings analogy), and the influence of taking into account orthotropic properties that are often the result of additive manufacturing, especially when using the most popular FDM technique. In addition, the additively manufactured propellers will be characterized in order to measure their mechanical properties and compare them against the numerical experiments.

# 5. Contact Author Email Address

For further information, please contact J. García Tíscar < jorgarti@mot.upv.es>.

# 6. Copyright Statement

The authors confirm that they, and/or their company or organization, hold copyright on all of the original material included in this paper. The authors also confirm that they have obtained permission, from the copyright holder of any third party material included in this paper, to publish it as part of their paper. The authors confirm that they give permission, or have obtained permission from the copyright holder of this paper, for the publication and distribution of this paper as part of the ICAS proceedings or as individual off-prints from the proceedings.

# **Acknowledgments**

This work was partly sponsored by grant PID2022-142018OA-I00 *Experimental and Numerical Optimization to Lower UAV Acoustical pollution (ENOLA)* funded by MCIN/AEI/10.13039/501100011033. F. N. Ramírez is supported by grant PREP2022-000221 funded by MCIN/AEI/10.13039/501100011033 and by "ESF Investing in your future".

#### References

- [1] Single European Sky ATM Research. European Drones Outlook Study, 2016. Last accessed: 2022-01-
- [2] Andrew Hately, A Van Swalm, A Volkert, A Rushton, A Garcia, C Ronfle-Nadaud, C Barrado, D Bajiou, D Martin, DD Vecchio, et al. U-space concept of operations. In *CORUS D6. 3, Ed. 03.00. 02*. SESAR Joint Undertaking, 2019.
- [3] Ministerio de Fomento, Gobierno de España. Plan Estratégico para el desarrollo del sector civil de los drones en España 2018-2021, 2018. Last accessed: 2023-06-23.
- [4] McKinsey & Company. Study on the societal acceptance of urban air mobility in europe. EASA report, American Institute of Aeronautics and Astronautics, July 2021.
- [5] World Health Organization. Regional Office for Europe. Burden of disease from environmental noise: quantification of healthy life years lost in Europe, 2011. Last accessed: 2023-04-12.
- [6] Andrew Christian and Randolph Cabell. Initial investigation into the psychoacoustic properties of small unmanned aerial system noise. 06 2017.
- [7] Marie Paul Nisingizwe, Pacifique Ndishimye, Katare Swaibu, Ladislas Nshimiyimana, Prosper Karame, Valentine Dushimiyimana, Jean Pierre Musabyimana, Clarisse Musanabaganwa, Sabin Nsanzimana, and Michael R Law. Effect of unmanned aerial vehicle (drone) delivery on blood product delivery time and wastage in rwanda: a retrospective, cross-sectional study and time series analysis. *The Lancet Global Health*, 10(4):e564–e569, 2022.

#### Effect of popular additive manufacturing technologies on the performance and acoustics of UAV propellers

- [8] Henry A Colorado, Carlos A Cardenas, Elkin I Gutierrez-Velazquez, Juan P Escobedo, and Sergio Neves Monteiro. Additive manufacturing in armor and military applications: research, materials, processing technologies, perspectives, and challenges. *Journal of Materials Research and Technology*, 2023.
- [9] Cesar Chavez-Tolentino, Zinrong Li, Hector R. Siller, and Hamid Sadat. Aerodynamic behavior and acoustic signature of propellers fabricated by additive manufacturing. *International Journal of Advanced Manufacturing Technology*, 129:3403–3412, 12 2023.
- [10] Christopher Thurman, D. Douglas Boyd Jr., Pieter Buning, Gabriel Reboul, and Christophe Benoit. Nasa/onera collaboration on small hovering rotor broadband noise prediction using lattice-boltzmann method and structured navier-stokes solvers. In 30th AIAA/CEAS Aeroacoustics Conference (2024).
- [11] José R. Serrano, Jorge García-Tíscar, Pedro Quintero, and Federico N. Ramírez. Numerical and Experimental Evaluation of Noise and Performance in UAV Propellers. volume Volume 1: Aircraft Engine of *Turbo Expo: Power for Land, Sea, and Air*, page V001T01A023, 06 2023.
- [12] AJ Torregrosa, A Gil, LM Garcia-Cuevas, P Quintero, and FD Denia. Prediction of the transmission loss in a flexible chamber. *Journal of Fluids and Structures*, 82:134–153, 2018.
- [13] AJ Torregrosa, A Gil, P Quintero, and A Tiseira. Enhanced design methodology of a low power stall regulated wind turbine. bemt and mrf-rans combination and comparison with existing designs. *Journal of Wind Engineering and Industrial Aerodynamics*, 190:230–244, 2019.
- [14] F. Möhren, O. Bergmann, F. Janser, and C. Braun. Assessment of structural mechanical effects related to torsional deformations of propellers. *CEAS Aeronautical Journal*, May 2024.